Many facets of modeling GW170817 kilonova

Oleg Korobkin
in collaboration with:
Ryan T. Wollaeger, Christopher J. Fontes, Stephan K. Rosswog,
Matthew R. Mumpower, Nicole Vassh, Wesley P. Even,
Christopher L. Fryer, Aimee L. Hungerford,
Gail McLaughlin, Rebecca Surman

FRIB and the GW170817 kilonova
East Lansing, MI

July 25, 2018

Los Alamos NATIONAL LABORATORY EST.1943

Approved for unlimited release
LA-UR-18-27532

r-Process nucleosynthesis calculations

The Nucleosynthesis and Decay of Heavy Elements:

rise

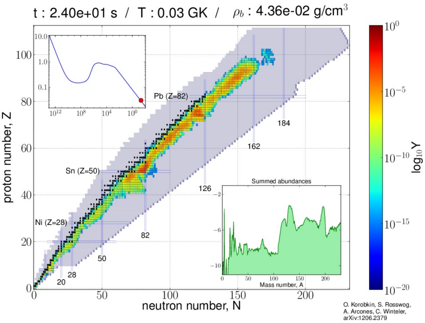

decay

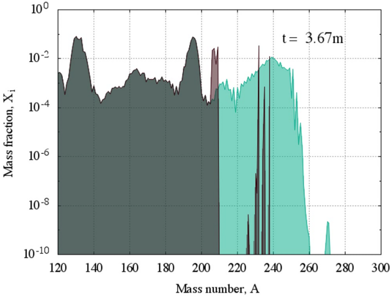

Kilonova: analytic estimates at peak

Peak times:

$$\tilde{t}_p \approx \sqrt{\frac{\kappa m_{\rm ej}}{4\pi c \bar{v}}} = \mathbf{4.9}\ \mathrm{days}\ \left(\frac{\kappa_{10} m_{\rm ej,-2}}{\bar{v}_{-1}}\right)^{1/2},$$

$$\tilde{L}_p \approx \dot{\epsilon}_0 m_{\rm ej} \left(\frac{\tilde{t}_p}{t_0}\right)^{-\alpha} = \mathbf{2.5 \times 10^{40}}\ \frac{\mathrm{erg}}{\mathrm{s}}\ \left(\frac{\varepsilon_{\rm th}}{0.5}\right)\ \left(\frac{\bar{v}_{-1}}{\kappa_{10}}\right)^{\alpha/2} m_{\rm ej,-2}^{1-\alpha/2},$$

$$\tilde{T}_{\rm eff} \approx \left(\frac{\dot{\epsilon}_0 c}{\sigma_{SB}}\right)^{1/4} \left(\frac{m_{ej}}{4\pi c t_0}\right)^{-\alpha/8} \kappa^{-(\alpha+2)/8} \bar{v}^{(\alpha-2)/8}$$

$$= \mathbf{2200}\ \mathrm{K}\ \kappa_{10}^{-(\alpha+2)/8} \bar{v}_{-1}^{(\alpha-2)/8} m_{\rm ej,-2}^{-\alpha/8}.$$

where $\kappa_{10} = (\kappa/10\,\mathrm{cm^2 g^{-1}})$, $m_{\rm ej,-2} = (m_{\rm ej}/0.01\,M_\odot)$, $\bar{v}_{-1} = (\bar{v}/0.1\,c)$, and $\alpha = 1.3$.

Very high opacities! (*Kasen, Badnell & Barnes 2013*, *Fontes+ 2015*).

NOTE: Bolometric luminosity is directly proportional to the effective nuclear heating.

Radioactive heating power

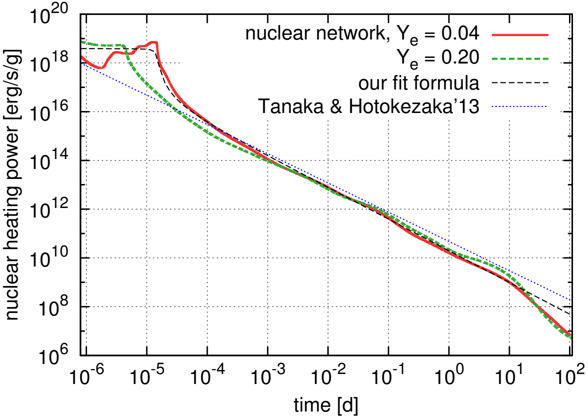

$$\dot{\epsilon}(t) = \left(\frac{\varepsilon_{\rm th}}{0.5}\right) 9.8 \times 10^{9}\ \mathrm{erg/(g \cdot s)} \left(\frac{t}{1\ \mathrm{day}}\right)^{-\alpha}, \quad \alpha \approx 1.3$$

GW170817: directly constraining nuclear heating

Comparing bolometric light curve from kilonova GW170817 with theoretical nuclear heating rates: electron fraction $Y_e \leq 0.3$.

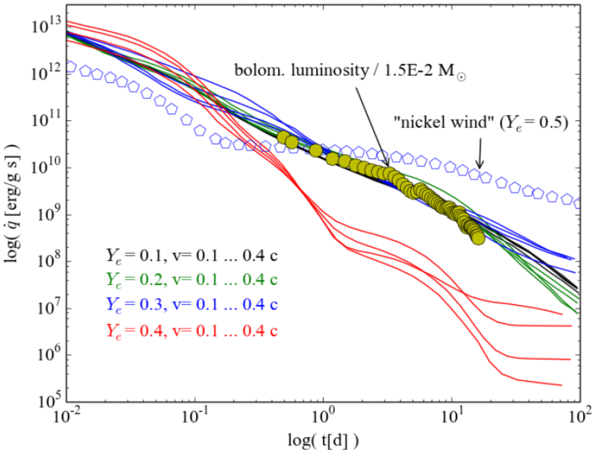

Rosswog et al., A&A (2018), "The first direct NSM detection ..."

Spherically-symmetric radiative diffusion model

For self-simlarly expanding spherical outflows, the radiative transfer equation

$$\frac{DE}{Dt} - \nabla \cdot \left(\frac{c}{3\kappa\rho} \nabla E \right) + \frac{4}{3} E \nabla \cdot \vec{v} = \rho \dot{q}(t). \tag{1}$$

in spherical symmetry and for constant opacity κ

$$\frac{DE}{Dt} - \frac{1}{R^2 x^2} \left[\frac{c}{3\kappa\rho} x^2 E' \right]' + \frac{4E}{t} = \rho \dot{q}(t), \tag{2}$$

admits separation of variables,

$$E(x,t) = E_0 \left[\frac{t_0}{t} \right]^4 \psi(x) \phi(t), \quad \text{and} \quad \rho(x,t) = \rho_0 \left[\frac{t_0}{t} \right]^3 \varphi(x). \tag{3}$$

which allows to compute realistic semianalytic solutions for internal energy and radiative flux. (Pinto & Eastman 2000b, Rosswog et al.2018)

Comparison of semianalytic models vs RT code

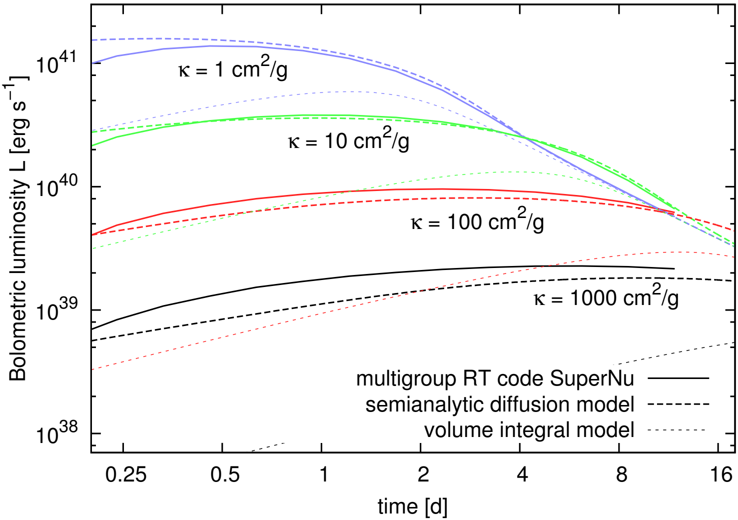

(Wollaeger et al. 2018, Rosswog et al. 2018)

Comparison of semianalytic models vs RT code

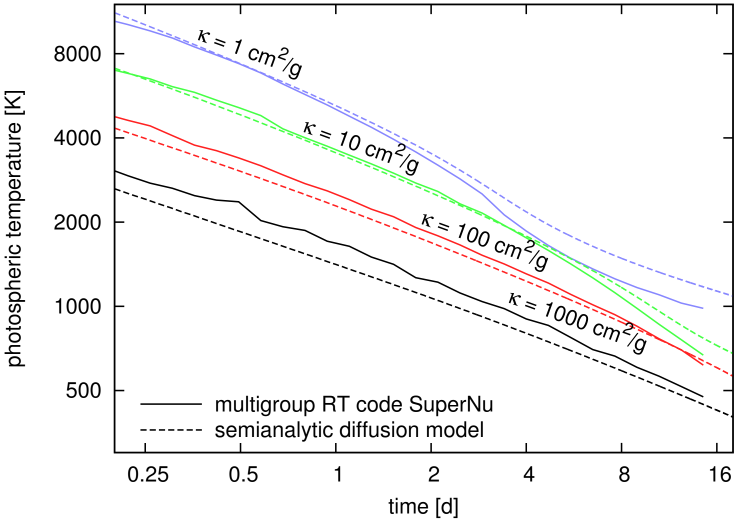

(Wollaeger et al. 2018, Rosswog et al. 2018)

Essential ingredient: partitioning of energy

Fraction of energy released with different decay products (FRDM):

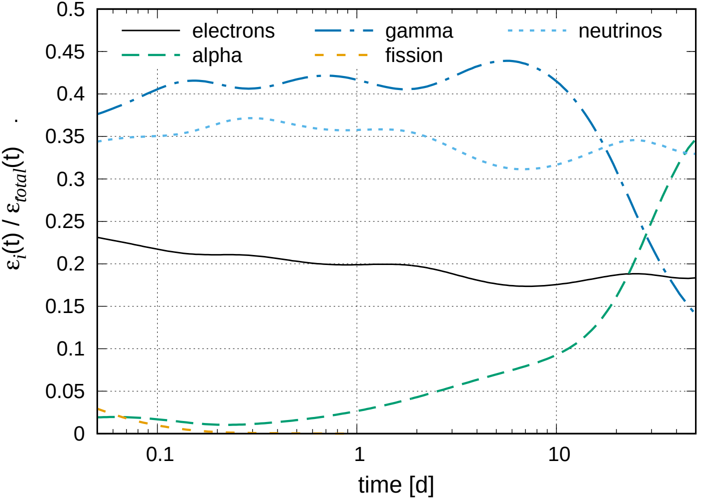

(Wollaeger et al. 2018)

Essential ingredient: thermalization

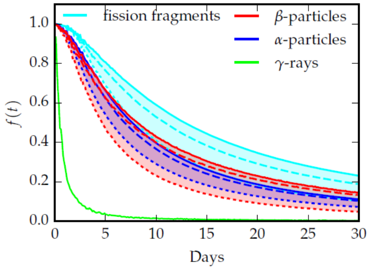

- time-dependent thermalization – see Barnes et al. (2016):

$$f_i(t,\mathbf{r}) = \frac{\log(1+2\eta_i^2)}{2\eta_i^2}, \quad (4)$$

$$2\eta_i^2(t,\mathbf{r}) = \frac{2A_i}{t\rho(t,\mathbf{r})}, \quad (5)$$

and the constants A_i determine thermalization times:
$\{A_\alpha,\ A_\beta,\ A_{\rm ff}\} = \{1.2,\ 1.3,\ 0.2\} \times 10^{-11}\mathrm{g\,cm^{-3}\,s}$
(Barnes et al. 2016).

Essential ingredient: effective nuclear heating

Effective nuclear heating rate comparison for the FRDM vs DZ31 nuclear mass models

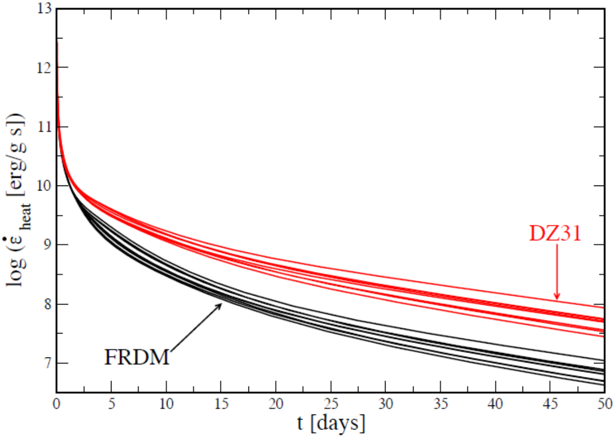

(Rosswog et al. 2017, Barnes et al. 2017):

Comparison with observations: g- and JHK-bands

Single-component constant-opacity semianalytic radiation diffusion model:

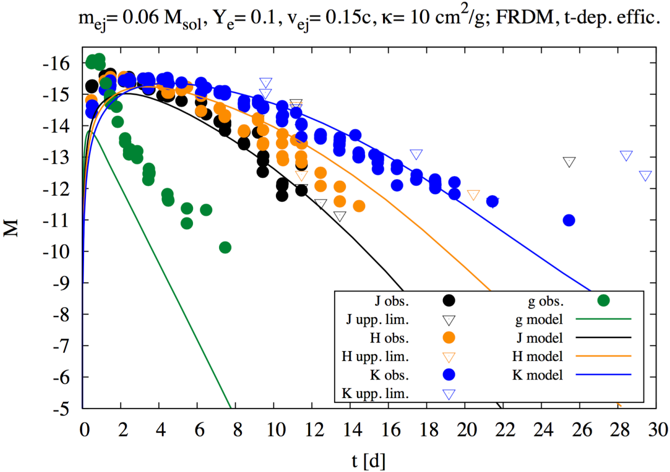

(Rosswog et al. 2018)

Comparison with observations: g- and JHK-bands

Single-component constant-opacity semianalytic radiation diffusion model:

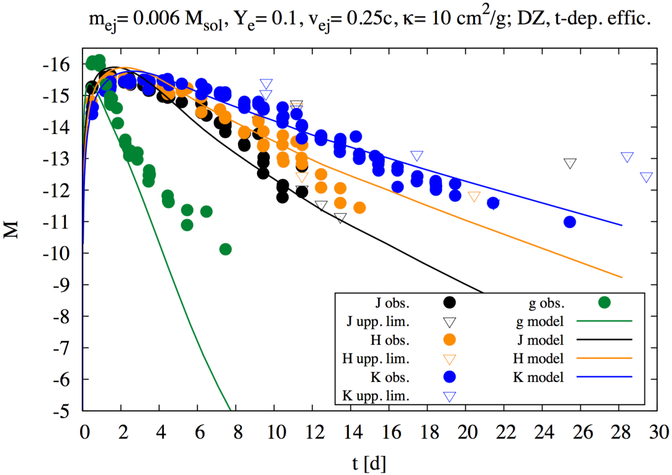

(Rosswog et al. 2018)

Can we observe individual decays?

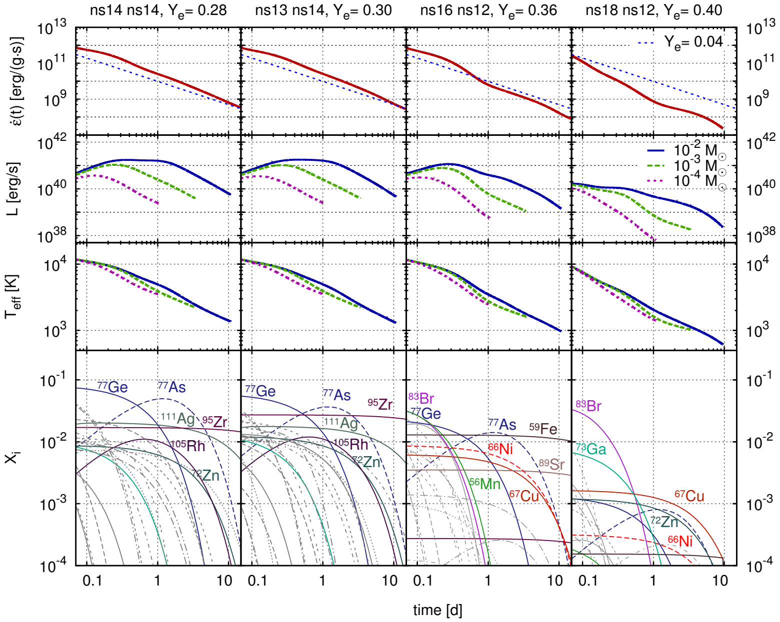

The imprint of ^{254}Cf on kilonova light curve:

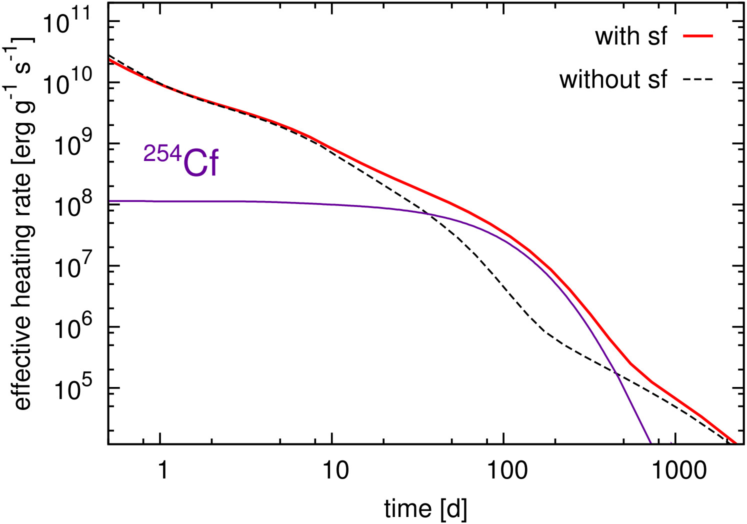

(Zhu et al., ApJL 2018)

The imprint of ^{254}Cf on kilonova light curve:

mass: 0.05 $M_\odot$, velocity: 0.1 c, $\kappa = 10\ \mathrm{cm^2 g^{-1}}$

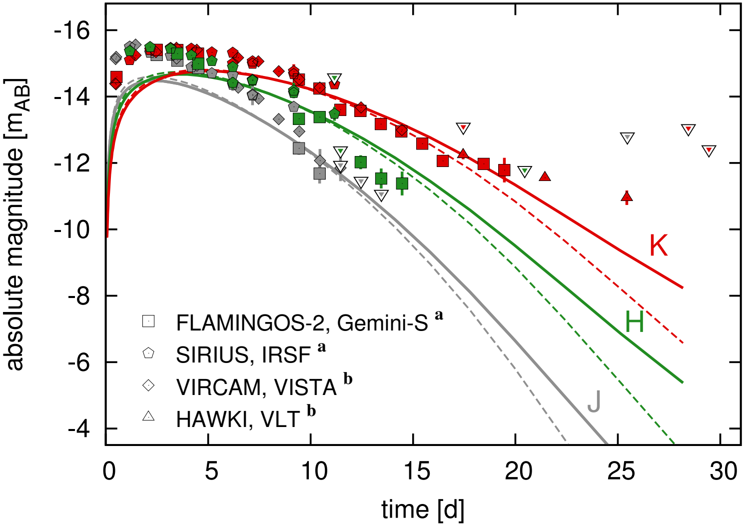

Simpler optically-thin model for late-time mid-IR

In *Zhu et al. (2018)*, we used a simpler model, following Li & Paczynski (1998) work. It results in following ODE (here, $\gamma \equiv 2 + c/v_{\rm ej}$ and $q_{\rm nuc}(t)$ is the effective nuclear heating rate):

$$\frac{d(aT^4)}{d\log t} = -\gamma a T^4 + \frac{q_{\rm nuc}(t)}{\kappa_P(T) v_{\rm ej}}. \qquad (6)$$

We adopted an approximate temperature dependence of the opacity:

$$\kappa_P(T) = 10\ \mathrm{cm}^2\ \mathrm{g}^{-1}\ \left(1 + \exp\left[\frac{1300\ K - T}{100\ K}\right]\right)^{-1}, \qquad (7)$$

capturing an exponential drop-off in the opacity as temperature drops below 1300 K and the plasma becomes neutral.

(Zhu et al., ApJL 2018)

Simpler optically-thin model for late-time mid-IR

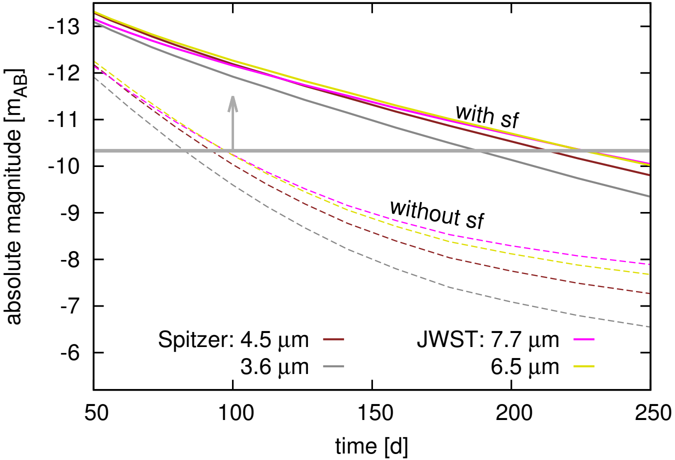

The gray horizontal line indicates JWST sensitivity threshold for mergers at 200 Mpc. (Zhu et al., ApJL 2018)

State-of-the-art models of kilonovae / macronovae

R. T. Wollaeger, O.K., C. J. Fontes, S. K. Rosswog, W. P. Even, C. L. Fryer, J. Sollerman, A. L. Hungerford, D. R. van Rossum, A. B. Wollaber,
"Impact of ejecta morphology and composition on the electromagnetic signatures of neutron star mergers",
MNRAS (2018)

Kilonova scenario

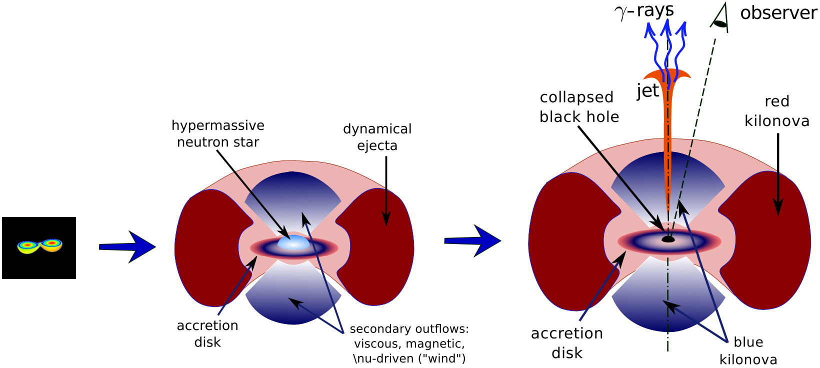

Multiple components are needed! (dynamical ejecta, ν-driven wind, accretion wind)

State-of-the-art: multicomponent models

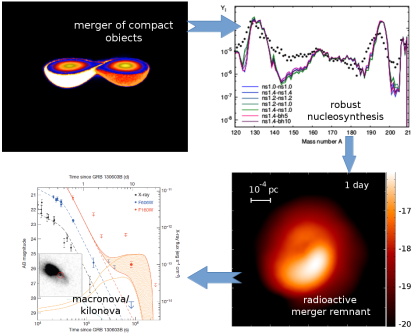

Necessary ingredients:

- multidimensional ejecta morphology;
- composition;
- nuclear heating;
- decay products;
- thermalization;
- opacities;
- radiative transfer.

Morphology and composition

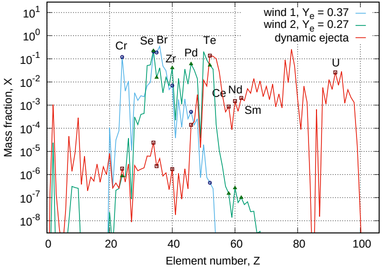

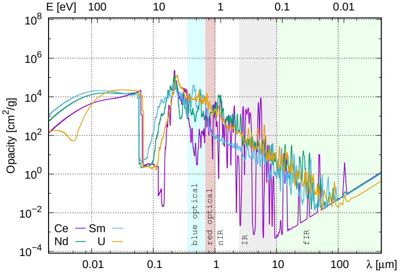

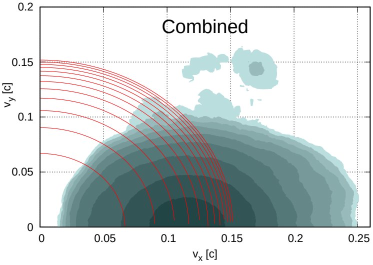

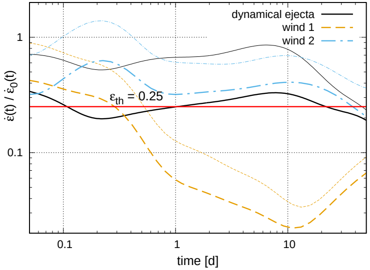

Morphology and composition

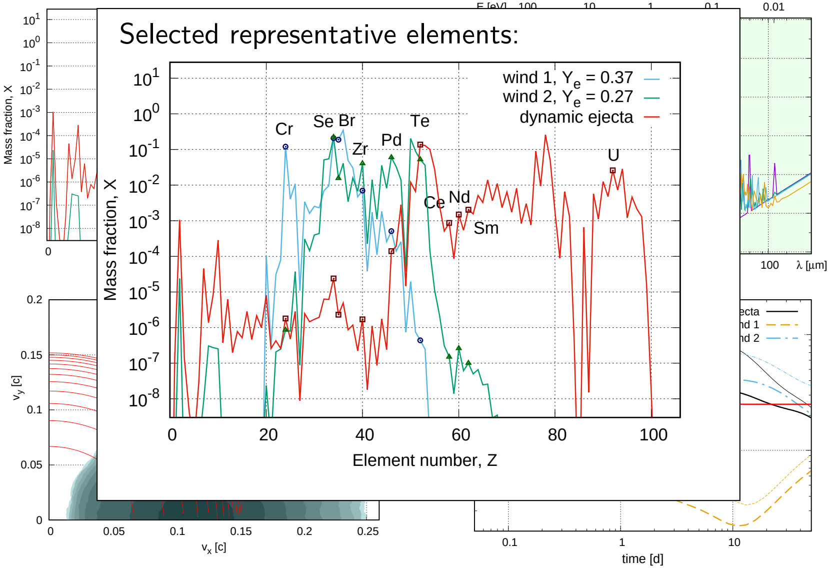

Morphology and composition

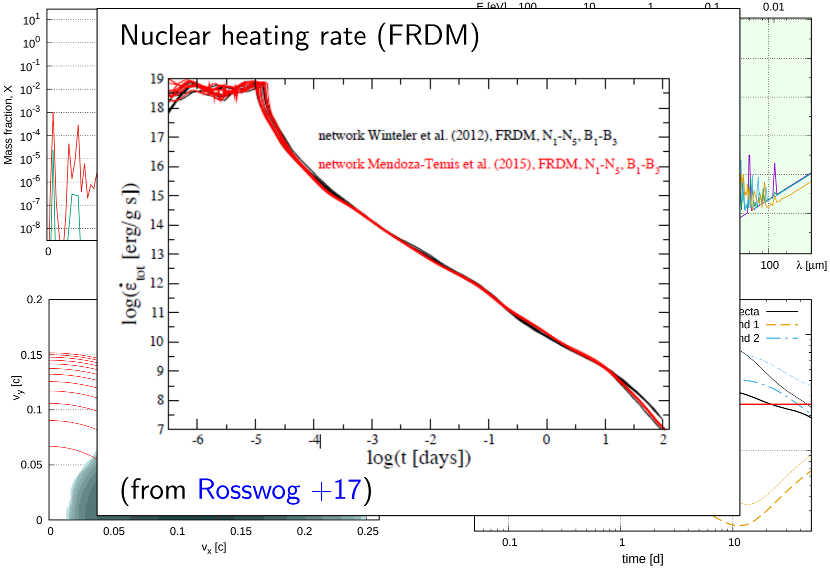

Morphology and composition

Fraction of energy released with different decay products (`WinNet`, FRDM):

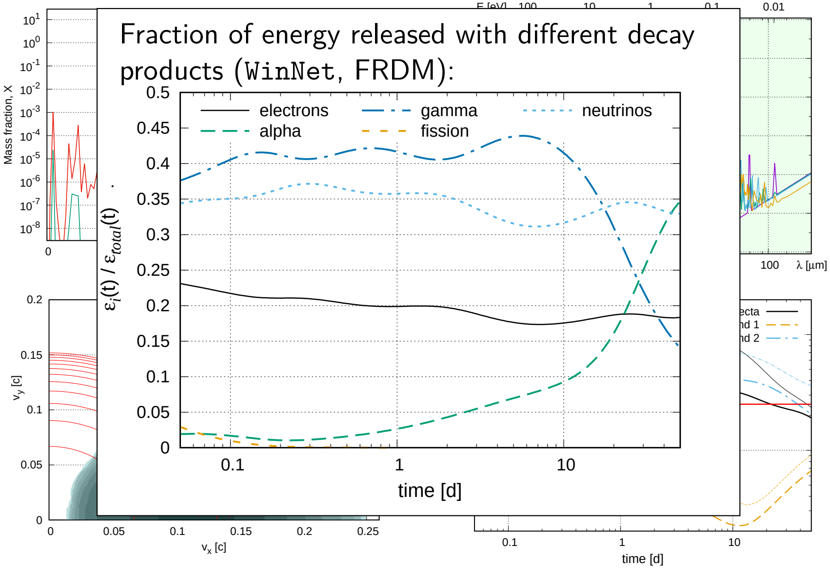

Morphology and composition

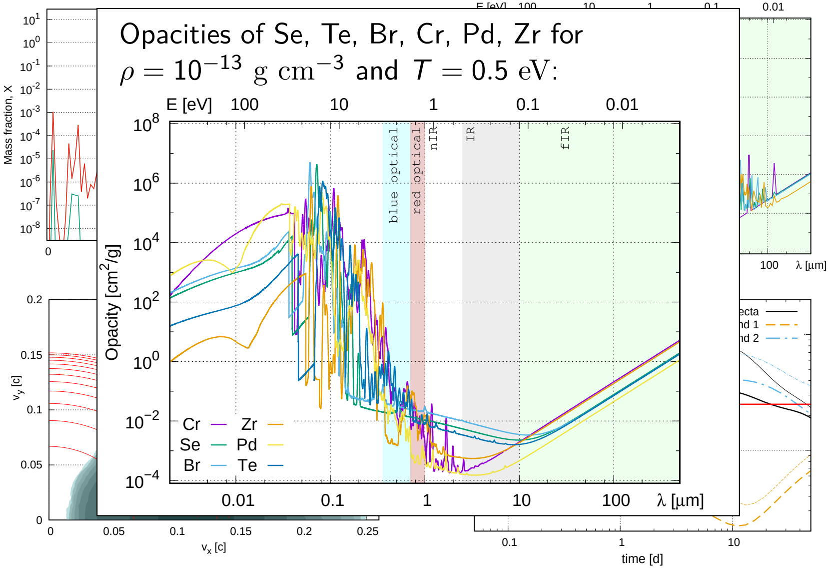

Morphology and composition

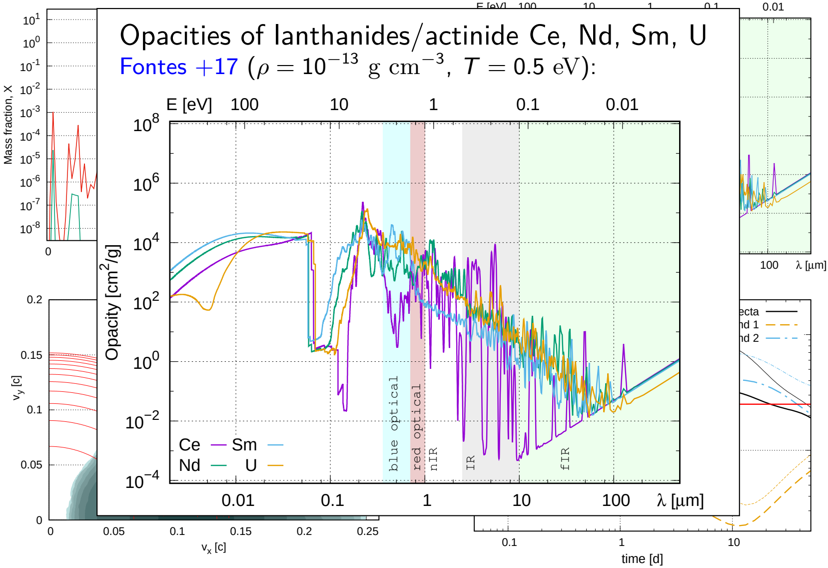

Radiative transfer: SuperNu

Features:

- multidimensional (1D, 2D axisymmetry, 3D);
- combines Implicit Monte Carlo (IMC) and Discrete Diffusion Monte Carlo (DDMC);
- background flows: partially-ionized multicomponent plasma;
- expansion: homologous approximation, $\vec{v} = \vec{r}/t$;
- first-order relativistic corrections (up to $O(v/c)$);
- opacity: 100-1000 log-spaced wavelength groups in comoving frame, from 10 nm to 3.2 μm;
- see Wollaeger and van Rossum, ApJS (2014);
- open source code, can be downloaded at: `https://bitbucket.org/drrossum/supernu/wiki/Home`

Results: synthetic spectra, blue vs red

- spectra depend on the type of open shell in electronic configuration: *p*-shell (Se, Br, Te), *d*-shell (Zr, Pd, Cr), or *f*-shell (Ce, Nd, Sm, U).

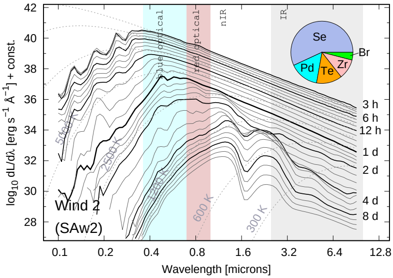

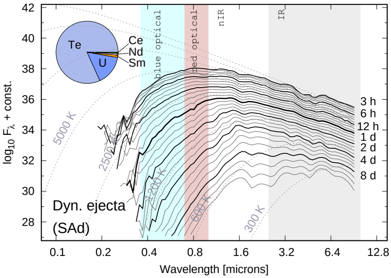

Results: 2D model

Spectra – effect of "lanthanide curtain":

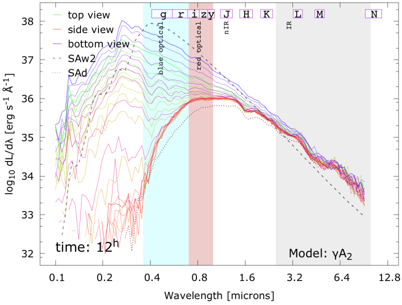

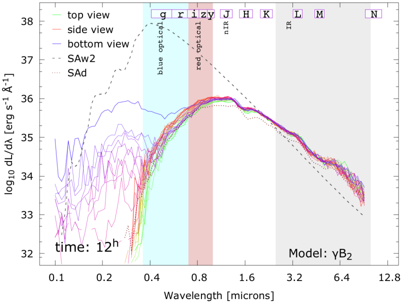

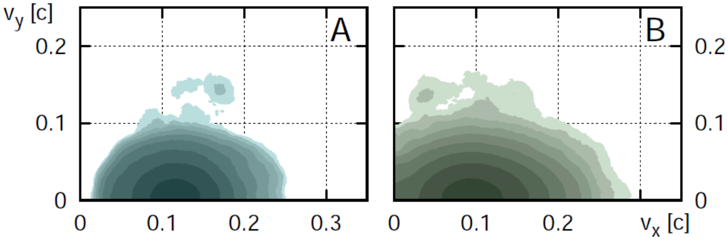

Results: 2D model

Spectra – effect of "lanthanide curtain":

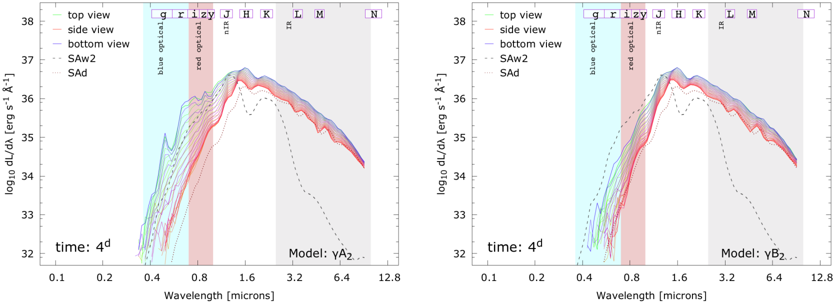

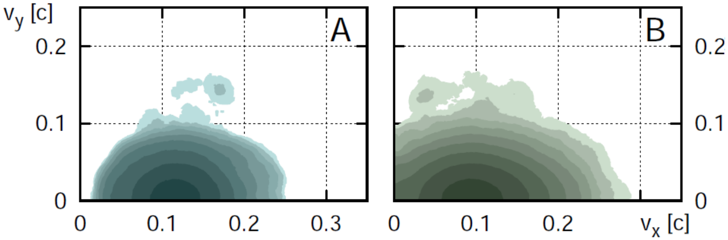

Early UV/optical emission: neutron richness

- iron-group only outflow is insufficient to explain the blue component;

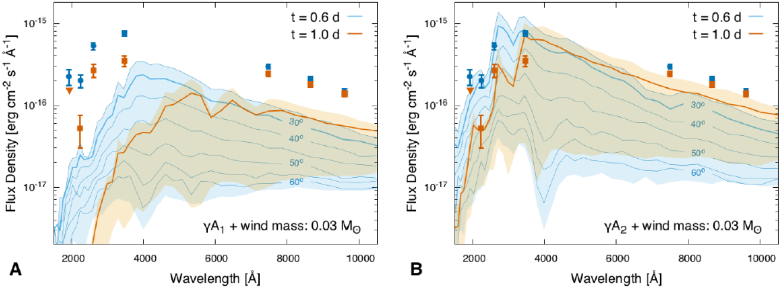

Figure S3: **The effect of wind electron fraction on the SED.** These SEDs have the same velocities and masses of the ejecta but different composition: "wind 1" (A) with abundant iron-group and the *d*-shell elements vs. "wind 2" (B) with the first peak elements, largely representing the *s*- and *p*-shell elements and relatively fewer *d*-shell elements. Notation for the plots is the same as in the previous figure. The iron-group dominated composition not only exhibits lower brightness but also shows much more reddening in the spectrum between the two epochs. Datapoints are as in Figure S2.

Evans et al. (2017), "Swift and NuSTAR observations of GW170817":

Hubble Optical and IR observations: inclination

- massive, high-speed wind along the polar axis ($M_{\rm wind} \sim 0.015\ M_\odot$, $v \sim 0.08c$), and lighter contibution from the dynamical ejecta ($M_{\rm dyn} \sim 0.002 M_\odot$, $v \sim 0.2c$), with viewing angle $\theta \sim 28^\circ$.
- models for X-ray afterglow and off-axis blue kilonova agree;

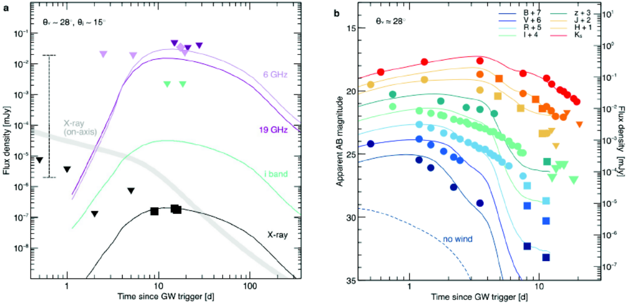

Figure 3: Multi-wavelength light curves for the counterpart of GW170817

Troja et al. (2017), "The X-Ray Counterpart to GW170817":

Application to GW170817: presence of lanthanides

- presence of lanthanide-rich component is crucial for explaining both optical and IR components;

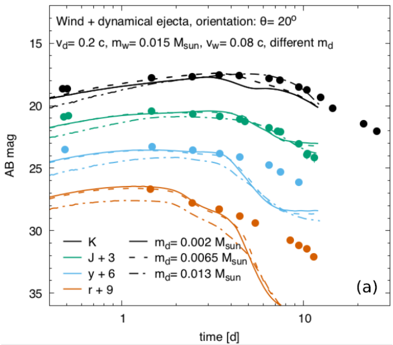

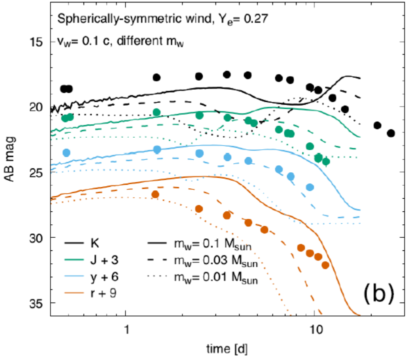

Tanvir et al. (2017), "The emergence of a lanthanide-rich kilonova"

Parameters of GW170817 from UV/optical/IR observations:

- **wind** composition: first r-process peak;
- wind mass: $m_{\rm wind} = 0.03 - 0.1 M_\odot$;
- wind velocity: $v_{\rm wind} = 0.08c$;
- wind kinetic energy: $E_{\rm wind} = 2 \times 10^{50} erg$;
- **dynamical ejecta** mass: poorly constrained, compatible with the range $m_{\rm dyn} = 0.002 - 0.03 M_\odot$;
- dynamical ejecta velocity: $v_{\rm dyn} = 0.2 - 0.3c$;
- dynamical ejecta kinetic energy: $E_{\rm dyn} = 6 \times 10^{50} erg$;
- **viewing angle**: $< 40^\circ$, degenerate with the wind outflow mass: higher polar angle implies higher mass, or non-axisymmetric configuration without dynamical ejecta obscuring the wind.
- **in agreement** with the masses and velocities found by other groups (Kawaguchi et al. (2018), Chornock et al. (2017)).

Implications for the r-process in the Milky Way

- NSM origin of heavy elements is consistent both with the statistical models of stellar populations, and with the models of galactic chemolution in the Milky Way.

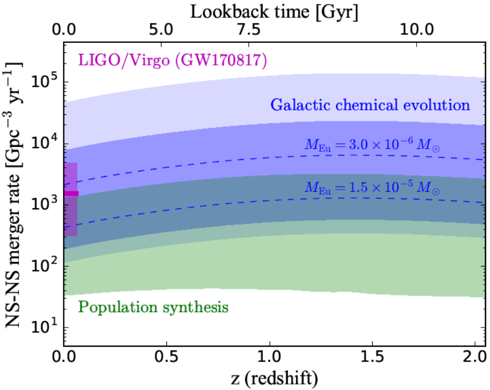

FIG. 2.— Neutron star - neutron star (NS-NS) merger rate density as a function of redshift. The two blue dashed lines show the

Côté et al. (2017), see also talk by Benoit;

GW170817: inferred masses

Mass estimates for high-opacity lanthanide-rich ($m_{\rm dyn}$) and medium-opacity material ($m_{\rm w}$), from recent literature:

Reference	$m_{\rm dyn}$ $[M_\odot]$	$m_{\rm w}$ $[M_\odot]$
Abbott +17	0.001 – 0.01	–
Arcavi +17	–	0.02 – 0.025
Cowperthwaite +17	0.04	0.01
Chornock +17	0.035	0.02
Evans +17	0.002 – 0.03	0.03 – 0.1
Kasen +17	0.04	0.025
Kasliwal +17	$>$ 0.02	$>$ 0.03
Kawaguchi +18	0.02	0.009
Nicholl +17	0.03	–
Perego +17	0.005 – 0.01	10^{-5} – 0.024
Rosswog +17	0.01	0.03
Smartt +17	0.03 – 0.05	0.018
Tanaka +17	0.01	0.03
Tanvir +17	0.002 – 0.01	0.015
Troja +17	0.001 – 0.01	0.015 – 0.03

(from Côté et al. 2017, "The Origin of r-Process Elements")

Conclusions and open questions

- high opacities imply **presence of lanthanides / actinides**;
- heating rates pattern – **lower limit on neutron richness**;
- paradigm shift: neutron star mergers might be **the main site of the r-process**.
- using 2D (3D) approach and multiple components is essential for correct numerical interpretation;
- secondary outflows ("wind") are rather more massive than previously estimated - **affected by neutrinos**;
- potentially observable imprint of ^{254}Cf fission (see talk by Matt).

Conclusions and open questions

- high opacities imply **presence of lanthanides / actinides**;
- heating rates pattern – **lower limit on neutron richness**;
- paradigm shift: neutron star mergers might be **the main site of the r-process**.
- using 2D (3D) approach and multiple components is essential for correct numerical interpretation;
- secondary outflows ("wind") are rather more massive than previously estimated - **affected by neutrinos**;
- potentially observable imprint of ^{254}Cf fission (see talk by Matt).
- **can the robustness of r-process help identify key reactions and nuclei for experimental studies?**
- **better RT models in optically thin regime;**
- **robust wind models – from accretion disk / HMNS;**
- **implications for high-density nuclear equation of state.**